Modeling a Dehalogenase Fold into the 8-Å Density Map for Ca^{2+}-ATPase Defines a New Domain Structure

David L. Stokes* and N. Michael Green†

*Skirball Institute of Biomolecular Research, Department of Cell Biology, New York University School of Medicine, New York, New York 10016 USA, and †National Institute for Medical Research, London NW7 1AA, England

ABSTRACT Members of the large family of P-type pumps use active transport to maintain gradients of a wide variety of cations across cellular membranes. Recent structures of two P-type pumps at 8-Å resolution have revealed the arrangement of transmembrane helices but were insufficient to reveal the architecture of the cytoplasmic domains. However, recent proposals of a structural homology with a superfamily of hydrolases offer a new basis for modeling these domains. In the current work, we have extended the sequence comparison for the superfamily and delineated domains in the 8-Å density map of Ca^{2+}-ATPase. The homology suggests a new domain structure for Ca^{2+}-ATPase and, specifically, that the phosphorylation domain adopts a Rossman fold. Accordingly, the atomic structure of L-2 haloacid dehalogenase has been fitted into the relevant domain of Ca^{2+}-ATPase. The resulting model suggests the existence of two ATP sites at the interface between two domains. Based on this new model, we are able to reconcile numerous results of mutagenesis and chemical cross-linking within the catalytic domains. Furthermore, we have used the model to predict the configuration of Mg·ATP at its binding site. Based on this prediction, we propose a mechanism, involving a change in Mg^{2+} liganding, for initiating the domain movements that couple sites of ion transport to ATP hydrolysis.

INTRODUCTION

In all cells, ionic homeostasis is maintained by members of the large family of P-type ion pumps (Axelsen and Palmgren, 1998). Ca^{2+}-ATPase and Na^+/K^+-ATPase are the two best-studied members, and they have been characterized in great detail with regard to reaction kinetics, chemical modification, and site-directed mutagenesis (Andersen, 1995; Moller et al., 1996; MacLennan et al., 1997). Structural studies by electron microscopy have recently culminated in structures at 8-Å resolution for both Ca^{2+}-ATPase (Zhang et al., 1998) and H^+-ATPase (Auer et al., 1998). These structures revealed similar arrangements of 10 transmembrane helices, and, in the case of Ca^{2+}-ATPase, connections were identified between four of these transmembrane helices and the corresponding stalk helices. In addition, a particular pathway for calcium through the transmembrane domain was proposed and the sequences of stalk and transmembrane helices were assigned, using a variety of constraints. Similar assignments were not possible for the cytoplasmic domains because they contain mainly β-strands and short helices, which are not easily identified at 8-Å resolution.

Nevertheless, based on secondary structure predictions and on functional considerations, a sophisticated model has evolved for the cytoplasmic portion of Ca^{2+}-ATPase, which includes the delineation of several domains (MacLennan et al., 1985; Taylor and Green, 1989; Green and Stokes, 1992). According to this model, the main cytoplasmic loop between transmembrane helices M4 and M5 begins with a phosphorylation domain that is separated from a nucleotide-binding domain by the dominant tryptic cleavage site (at R^{505}) and ends with a 60-residue "hinge" domain, which was postulated to fold back onto the phosphorylation domain to produce the tertiary fold. An alternative to these three sequential domains is a model in which the nucleotide-binding domain forms an insert relative to a combined phosphorylation/hinge domain. Although the sequential domain model was never entirely satisfactory, the alternative with an inserted domain was unusual and, at that time, was not supported by evidence for an insertion site.

However, Aravind et al. (1998) recently proposed the existence of a superfamily of HAD hydrolases that includes the P-type pumps and that specifically supports a model with an inserted nucleotide-binding domain. This superfamily is based on homology between the phosphorylation domains of the P-type ATPases and the catalytic domains of serine/threonine phosphatases, phosphoglycomutases, and haloacid dehalogenases (HADs). Besides the sequence homology, these families also share the use of an aspartyl ester intermediate (Collet et al., 1998), the dynamics of which, in the pumps, are closely linked to the occlusion and transport of cations across the membrane. Here we show how the proposed homology leads to a new domain structure for the P-type ATPases, which we correlate with domains identified in the cytoplasmic portion of the 8-Å density map for Ca^{2+}-ATPase. By fitting the crystal structure for a haloacid dehalogenase to this map, we propose a model not only of the phosphorylation domain, but also of the structural components coupling this domain with the ion transport sites within the membrane. This model provides insight into the

Received for publication 7 October 1999 and in final form 12 December 1999.

Address reprint requests to Dr. David L. Stokes, Skirball Institute of Biomolecular Research, Department of Cell Biology, New York University School of Medicine, New York, NY 10016. Tel.: 212-263-1580; Fax: 212-263-1580; E-mail: stokes@saturn.med.nyu.edu.

0006-3495/00/04/1765/12 $2.00

effects of site-directed mutation and chemical modification; it supports the existence of two overlapping nucleotide-binding sites, and it suggests a role for Mg^{2+} in initiating the conformational changes required for Ca^{2+} translocation.

RESULTS

Sequence alignment and domain structure of dehalogenases and P-type pumps

A homology between the L-2 haloacid dehalogenase from *Pseudomonas* sp. YL (1JUD) and P-type pumps was proposed by Aravind et al. (1998), based on four sequence motifs that contribute to the active sites of these divergent enzymes. We begin our comparison by reviewing evidence from a wide variety of sources that support this homology. The crystal structure of 1JUD reveals the existence of two distinct domains (Fig. 1) (Hisano et al., 1996), the core domain being an α/β sandwich with the topology of a Rossmann fold (β-strand order 3-2-1-4-5-6). The catalytic aspartate is at the C-terminus of β1 and is followed first by a five-residue coil (*cyan* in Fig. 1) and then by the inserted subdomain, which consists of a distorted four-helix bundle (*gray* in Fig. 1). The chain then returns to the first helix (α5) of the core domain and completes the Rossman fold. The sequence motifs involved in the proposed homology are in four of the loops at the top of the β-sheet (*red* residues in Fig. 1 *b*, including the catalytic aspartate and the cyan coil). According to mutagenesis studies (Kurihara et al., 1995) and the crystal structures of dehalogenases in the presence of a substrate analog (Li et al., 1998; Ridder et al., 1997), most of these conserved residues contribute directly to the active site. R^{41} is the only residue from the α-helical subdomain that is directly involved in dehalogenation and serves to stabilize and to abstract the halide (Ridder et al., 1997). This role suggests that the subdomain is primarily involved in substrate specificity and binding, which would explain its variability across the proposed superfamily.

We have expanded the original alignment of these four sequence motifs to encompass the entire sequence between M4 and M6. Fig. 2 compares the sequence from 1JUD with four representative P-type ATPases from three main subfamilies (Axelsen and Palmgren, 1998): the type I heavy metal ATPases (CadA), the type III plant and fungal H^+-ATPases (H-ATP), and the type II animal Na^+/K^+- and Ca^{2+}-ATPases (NaATP, CaATP). The sequences homologous to the dehalogenase core domain are referred to as the phosphorylation or P-domain and the inserted subdomain (140–240 residues in the ATPases) as the adenosine-binding or A-domain. The presence of this inserted subdomain in Ca^{2+}-ATPase is strongly supported by the recent isolation and characterization of a proteolytic fragment with termini (T^{357}-T^{608}) close to those of the putative A-domain (Champeil et al., 1998). Furthermore, this proteolytic fragment was shown to retain tertiary structure, to bind nucle-

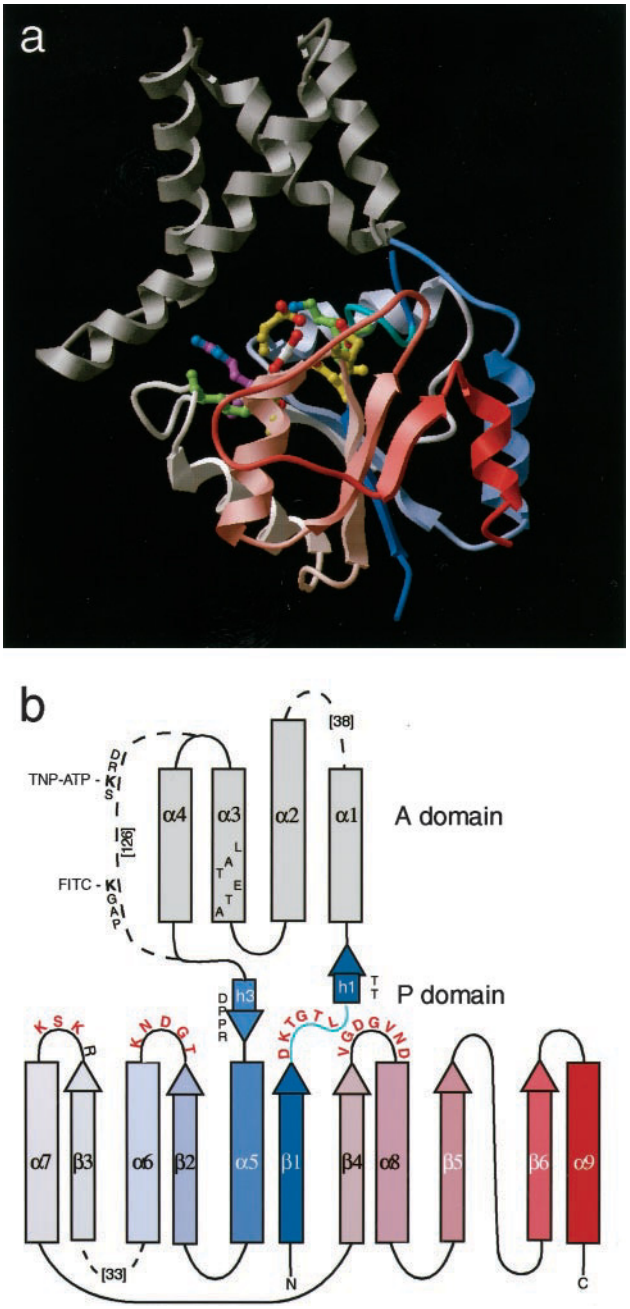

FIGURE 1 Structure of chloroacetate dehalogenase (1JUD). (*a*) This ribbon model was generated by ICM (Abagyan et al., 1994), using a pdb file of 1JUD, in which important functional residues were mutated by Quanta (MSI, San Diego, CA) to the corresponding residues of the sequence of the Ca^{2+}-ATPase (shown in *red* in *b*). The backbone of the Rossmann fold is color-coded from blue at the N-terminus to red at the C-terminus. The inserted four-helix subdomain is gray. Catalytic residues are colored as follows: Asp (351, 601, 703, 707) are yellow, Lys (352, 684) are green, Arg (678) is purple, the β_1-loop ($KTGTL^{356}$) is cyan, and VO_3^- is white. (*b*) The topology diagram shows the positions of three major inserts by Ca^{2+}-ATPase into the sequence of 1JUD (*dotted lines,* with the number of inserted residues in brackets). The largest insert replaces α4 in the A-domain and includes sites of TNP-ATP and FITC labeling (K^{492} and K^{515}). The two short strands that link the domains form a hinge and have been redesignated as *h1* and *h2*, and the strands of the β-sheet have been renumbered from β1 to β6. Residue numbers correspond to CaATPase.

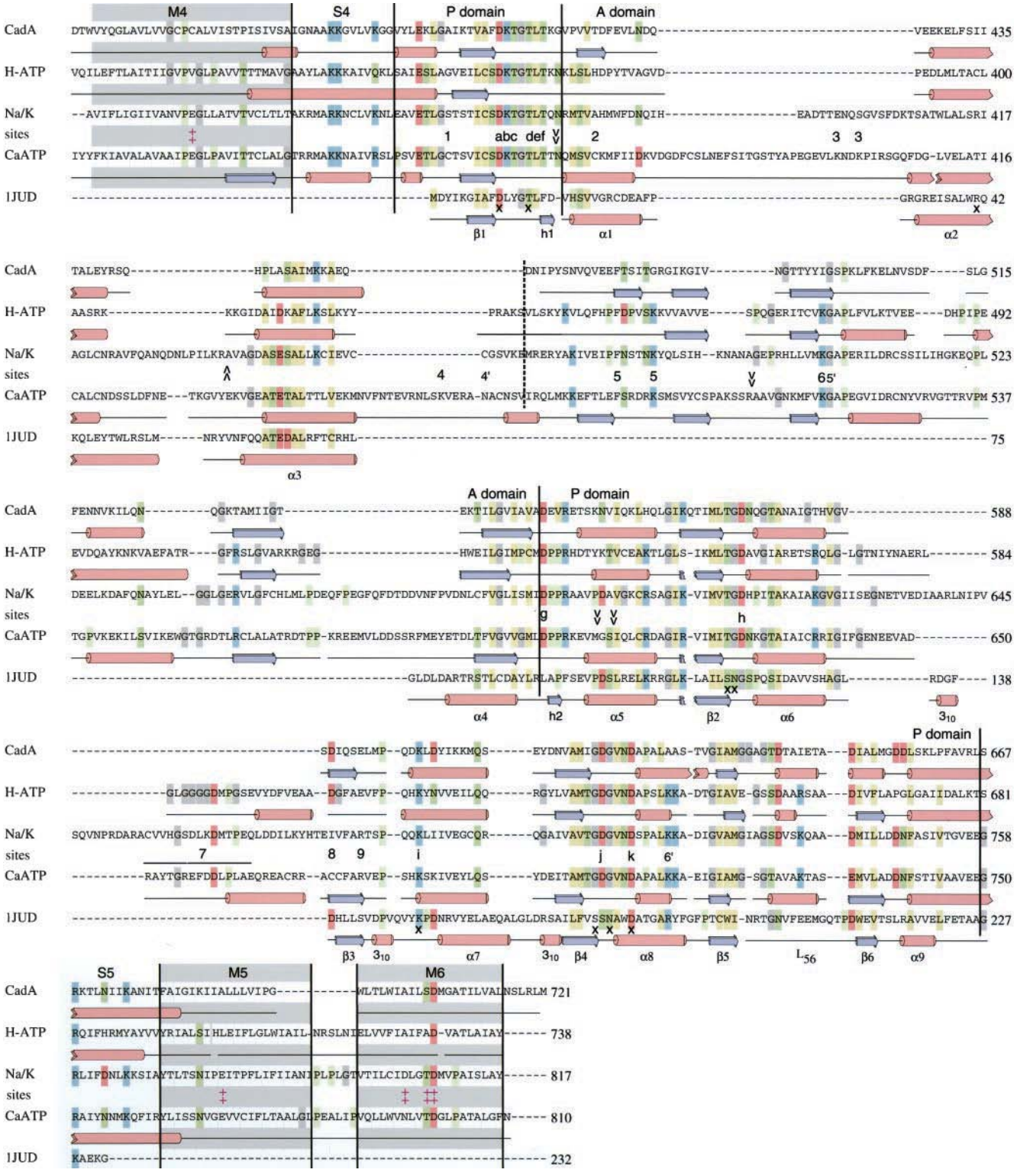

FIGURE 2 Alignment of the phosphorylation (P) and adenosine binding (A) domains of the ATPases with 1JUD. Four sequences of ATPases (SWISSPROT codes cada_staau, pma1_neucr, atn1_sheep, atcb_rabit) are aligned together with secondary structures predicted independently for three families by PHD (Rost and Sander, 1993). The predicted structure was used to supplement the sequence motifs and to guide the alignment to 1JUD. The A-domain has been divided at a conserved intron site (*dashed line*) into an N-terminal A1 region, with some similarity to 1JUD, and a C-terminal A2 region containing adenosine-binding sites, but with no resemblance to 1JUD. The intron sites for CadA and H-ATP were deduced from homologous positions of the Menkes Cu^{2+}-ATPase (Tumer et al., 1995) and the *Nicotiana* H^+-ATPase (Perez et al., 1992) genes. Sites of chemical labeling (1–9), mutation (a–j), proteolysis ($\gg$) and Ca^{2+} binding (++) are shown for the Ca^{2+}-ATPase. Many of these sites are also relevant to Na^+/K^+-ATPase, but three unique sites

TABLE 1 Functional Sites of the Na^+/K^+-ATPase and Ca^{2+}-ATPase

Site		Label	Domain	Activity				Ref.
				ATPase	E_1P	AcPase	E_2P	
Ca^{2+}-ATPase								
1	C344	ANSmal	P: β1	+	+	+	+	Bigelow and Inesi (1992)
		NBDCl						"
2	C364	ANSmal	A1	+	+	+	+	"
3	K394	Phospholamban*	A1					James et al. (1989)
	K400							
4	K464	ErITC	A1	0.2*	+	+	+	Huang et al. (1998)
5	K492	PAL	A2	−	−	+	+	McIntosh (1998)
		ADPpal		−	−			"
		TNPAzATP		−	−	+	+	"
		AMCA		+	+	+	+	"
		Glutarald.*		−	+	E_1P	−	"
6	K515	FITC	A2	−	−	+	+	Murphy (1988)
7	651–665	A52 antibody	P: α6-β5					McIntosh (1998)
8	C674	IAF	P: β3	+	+	+	+	Bigelow and Inesi (1992)
		IAEDANS						
9	R678	Glutarald.*	P: β3	−	+	E_1P	−	McIntosh (1998)
i	K684	ADPpal/Ca	P: β3-α7	−	−			"
Na^+/K^+-ATPase								
4′	C457	IAF	A1	+	+	+	+	"
5′	G502	AzATP	A2	0.5*	−			Tran et al. (1994)
5	K480	TNPAzADP	A2	−	−	+	+	Ward and Cavieres (1998b)
j	D703	ClRATP	P: β4-α8	−	−			McIntosh (1998)
k	D707	ClRATP	P: α8	−	−			"
6′	K719	FSBA	P: α8	−		+		"

Site designations refer to Fig. 2, where primes relate exclusively to the Na^+/K^+-ATPase and lowercase letters refer to sites that have also been mutated and therefore also appear in Table 2. The A-domain has been subdivided into A1 and A2 by the intron site in Fig. 2, and elements of secondary structure within the P-domain refer to the Rossman fold of 1JUD in Fig. 1. The catalytic and phosphorylation characteristics are given approximately as + (normal) and − (<10% active); when more complex effects are observed (*) the original papers should be consulted. ATPase and AcPase indicate hydrolysis of ATP and acetylphosphate, respectively; E_1P and E_2P indicate formation of phosphoenzyme from ATP and P_i, respectively. Most references are to two major reviews. ADPpal, pyridoxal-5′-diphosphoadenosine; AMCA, 7-amino-4-methylcoumarin-3-acetic acid; ANSmal, 2-(4-maleimidoanilino)naphthalene-6-sulfonate; AzATP, 8-azido-ATP; ClRATP, γ-(4-*N*-2-chloroethyl-*N*-methylamino)-benzylamide-ATP; ErITC, erythrosin-5′-isothiocyanate; FITC, fluorescein-5′-isothiocyanate; FSBA, 5′-(4-fluorosulfonylbenzoyl) adenosine; IAEDANS, *N*-iodoacetyl-*N*′-(5-sulfo-1-naphthyl)ethylenediamine; IAF, 5′-iodoacetamidofluorescein; NBDCl, 7-chloro-4-nitrobenzo-2-oxa-1,3-diazole; PAL, pyridoxal-5′-phosphate; TNPAzATP, 2′,3′-*O*-trinitrophenyl-8-azido-adenosine triphosphate.

otides, and to react specifically with fluorescein isothiocyanate (FITC), supporting its proposed functional role in binding nucleotide. The independently predicted secondary structures of the P-domains are consistent both with each other and with the crystal structure of 1JUD. The only significant disparities are a variable insert following α6 and some differences in the loop between β5 and β6 (which is the site of a two-helix insert in the dehalogenase from *Xanthobacter autrophicus*; Ridder et al., 1997). In view of the low overall sequence identity (8–14%), further support was obtained from the structure-based GenTHREADER program, which picked 1JUD from the structure database as the only certain match ($p = 1$) to any of the ATPases in Fig. 2 (N. M. Green and J. Saldanha, unpublished observations). All together, these results provide firm ground for fitting the structure of the 1JUD core domain into the 8-Å density map of Ca^{2+}-ATPase, which we describe below.

Given the dissimilarity of their substrates, it is not surprising that the subdomain of 1JUD differs from the A-domains of the pumps, which are all much larger. Nevertheless, near the N-terminus of the A-domain in Ca^{2+}-ATPase there are three predicted helices that could parallel those of 1JUD, one of which (α3) includes a notable sequence similarity (EATETAL/QATEDAL). In 1JUD these three helices are reconnected to the core domain by a fourth helix, whereas in the pumps, this connection expands to form a region of mixed secondary structure, including sites labeled by FITC and by azido-adenosine nucleotides (Figs. 1 *b* and 2). These differences in homology and secondary structure as well as the existence of a conserved intron site (*dashed*

for Na^+/K^+-ATPase are designated with primes (4′, 5′, and 6′). These sites are characterized in more detail in Tables 1 and 2. Finally, residues directly involved in the catalysis of 1JUD are indicated by x's below their sequence.

line in Fig 2; McIntosh, 1998) suggest that the A-domain may be subdivided into two parts (A1 and A2).

The proposed functional distinction between the P- and A-domains is supported by the effects of site-directed mutagenesis and chemical modification of Ca^{2+}-ATPase and Na^+/K^+-ATPase (Tables 1 and 2). ATP analogs with reactive groups on the ring invariably label residues in the A-domain (sites 4, 5, 5′, 6); as a result, these analogs block ATP-activated phosphorylation and transport, but not hydrolysis of acetyl phosphate or phosphorylation by P_i. In contrast, reactive groups near the γ-phosphate label residues in the P-domain (sites 6′, j, k); the modified ATPases are completely inactive and phosphorylation either by ATP or by P_i is blocked. Similarly, mutations of residues in the A-domain (sites 5, 5′, and 6) have much smaller effects on activity than do those in the P-domain (sites a–k), and the mutations at site 5 are the only ones with specific effects on ATP binding (McIntosh et al., 1996).

Domain boundaries in the density map

These considerations suggest that the cytoplasmic part of Ca^{2+}-ATPase is made up of three domains: the A- and P-domains for the loop between M4 and M5 and the "β-domain" for the loop between M2 and M3, which is predicted to be predominantly β-strand (Green and Stokes, 1992). We have therefore looked for these three domains in the cytoplasmic portion of our Ca^{2+}-ATPase density map (Fig. 3). The transmembrane and stalk regions had previously been fitted with α-helices (Zhang et al., 1998), and we therefore considered only the densities between the top of the stalk and the top of the molecule. In particular, we examined the map for low-density regions that might represent boundaries between domains, both in contour plots of map sections (Fig. 3, *d–f*) and in surface representations of the molecule (Fig. 3, *a–c*). The molecular surface depends on the density level that is chosen, and the figure shows the cytoplasmic region at a relatively high density threshold, with three domains (colored yellow, orange, and blue). The boundaries of the yellow domain were the best defined and delineate a block-like domain that sits on top of the stalk. On the other hand, the boundary between orange and blue domains was unclear, and we have left the corresponding part of the surface uncolored in this region. Contour plots correspond to cross sections through a dimer, with domains outlined on one of the two protomers.

According to the homology with dehalogenases, the P-domain composing the Rossman fold begins and ends only a few residues from the ends of stalk helices S4 and S5, respectively, so it was logical to assign it to the yellow domain in Fig. 3. Indeed, the volume of this yellow domain corresponds closely to the expected mass of the P-domain (Table 3), leading us to fit the atomic coordinates for 1JUD (see next section). The nucleotide is expected to bind at the interface between the P-domain and the A-domain, which is consistent with the previously defined site of CrATP binding (Yonekura et al., 1997). Although the 14-Å resolution of the CrATP difference map was insufficient to define boundaries, the CrATP difference density lies on the boundary between the orange and yellow domains (# in Fig. 3 *a* and *arrow* in Fig. 3 *d*). This suggests that the orange domain corresponds to the A-domain and that the blue domain corresponds to the β-domain

Two very high densities are apparent in Fig. 3 *f*, which we believe are good candidates for the decavanadate used to induce crystallization. One of these is present on the dyad axis (* in Fig. 3 *f*), and, given its position on a symmetry axis, it is unlikely to represent protein. The peak is ~10 Å in diameter and is therefore the right size and shape for a decavanadate ion (Day et al., 1987). Accordingly, this peak

TABLE 2 Mutation-sensitive sites of Ca^{2+}-ATPase

Site	Mutant	Domain	Type	Site	Mutant	Domain	Type
a	D351-N	P: β1	P−	5	F487-S	A2	Katp oc−
	-T		P−	5	K492-Y	A2	Katp oc−
				6	K515-E	A2	slow
b	K352-R	P: L	P−	g	D601-E	P: h2	P−
	-Q		P−		-N		E_1P
c	T353-A	P: L	E_1P	h	D627-A	P: β2-α6	P−
	-S		Slow		-N		E_1P
d	T355-A	P: L	Slow	i	K684-R	P: β3-α7	E_1P
	-S		WT		-H		P−
e	L356-T	P: L	Slow	j	D703-A	P: β4-α8	P− oc+
	-I		WT	k	D707-A	P: α8	P−
f	T357-A	P: h1	P−				
	-S		WT				

Most of the mutants in the P- and A-domains that have large effects on activity are shown and most are in the P-domain; the A-domain has been subdivided into A1 and A2 by the intron site. The corresponding lowercase letters are shown in Fig. 2. The elements of secondary structure for the P-domain refer to the proposed Rossman fold in Fig. 1. The effects of mutagenesis are classified according to the nomenclature of Andersen (1995), which provides a general review: P−, no phosphorylation from MgATP or from P_i; E_1P, transition from E_1-P · Mg · Ca_2 to E_2MgP_i is blocked; Slow, cycle is normal except that the transport rate is slow; oc−, unable to occlude Ca^{2+} with CrATP; WT, cycle is normal.

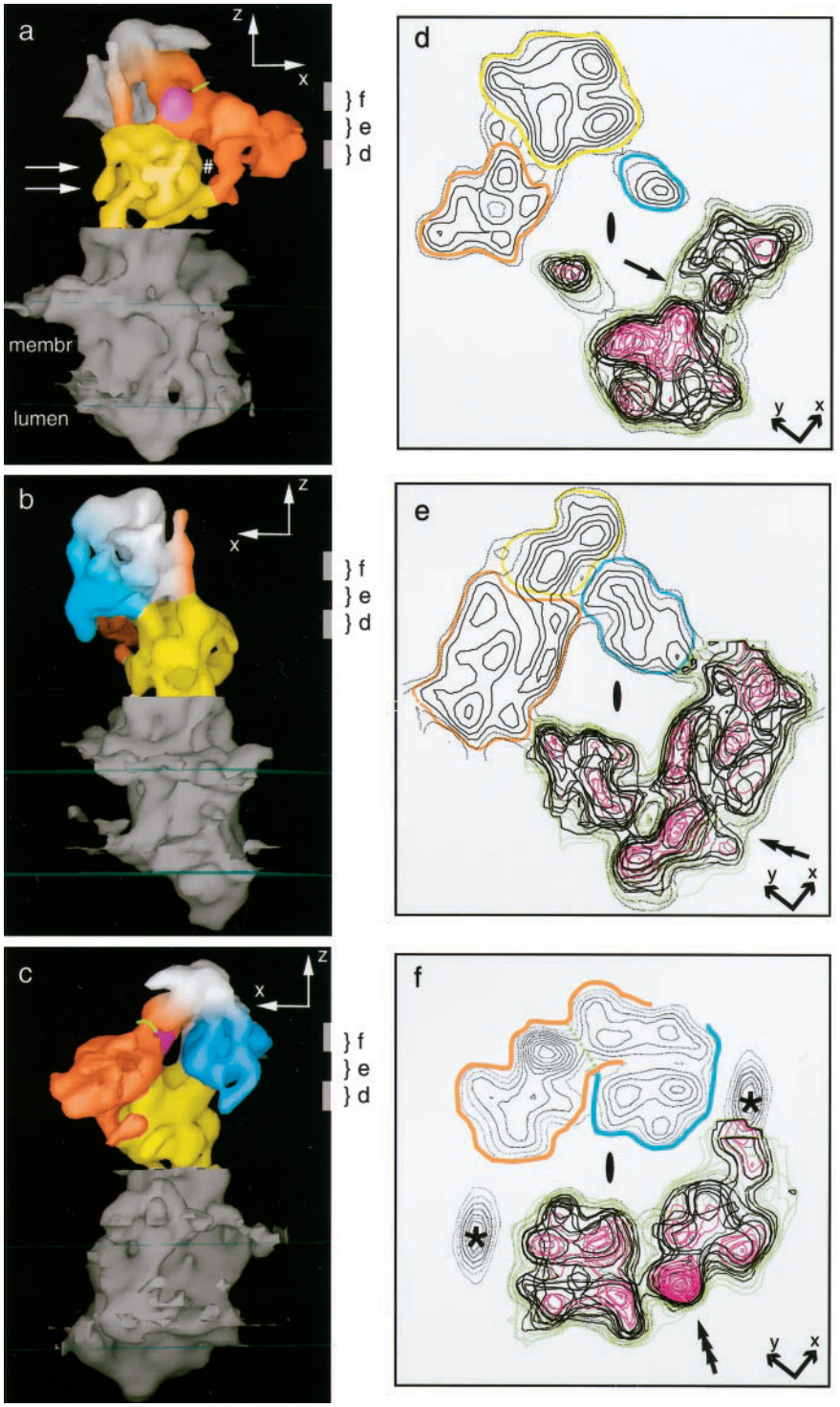

FIGURE 3 Domains in the cytoplasmic region of Ca^{2+}-ATPase. (*a–c*) Surface representation of the density map in which the three domains composing the cytoplasmic head have been contoured at a higher density and colored. Yellow corresponds to the P-domain, orange to the A-domain, blue to the β-domain, and purple to the putative decavanadate site; the green line indicates a possible delineation between the two parts of the A-domain. Domain boundaries were difficult to discern at the top of the molecule, which has therefore been left uncolored. The molecule is shown in three orientations related by ~90° rotations about the vertical (*z*) axis. The three zones indicated at the right margins correspond to the sections shown in *d–f*. The white arrows on the left correspond to the levels shown in Fig. 4, *a* and *c*. (*d–f*) Sections through two molecules related by a twofold axis, showing the low density boundaries between the three cytoplasmic domains. The colored contours represent a single molecule masked from the surrounding crystal lattice and correspond to four superimposed 2-Å-thick sections. Green, dashed contours are lowest, black are intermediate, and magenta are the highest density; thus, domain boundaries are likely to exist in regions filled with green contour lines. Twofold related molecules are represented by a single 2-Å section with only black contours, and the domains have been outlined in colors corresponding to those in *a–c*. The single arrow in *d* and # in *a* show the cavity occupied by Cr-ATP (Yonekura et al., 1997). The double arrowhead in *e* indicates a deep, curved cavity that is postulated as a potential second nucleotide binding site. Densities corresponding to two proposed decavanadate binding sites are indicated in *f* by the asterisks and by the triple arrowhead; the latter is colored magenta in *a* and *c*.

was omitted from the molecule in previous publications (Zhang et al., 1998; Toyoshima et al., 1993). Further examination of Fig. 3 *f* reveals a second peak of high density within the A-domain, which is much higher than that from an α-helix (magenta in Fig. 3, *a* and *c*; *triple arrowhead* in Fig. 3 *f*). Again, this peak is ~10 Å in diameter and may represent a second, internal site for decavanadate. If so, it would imply a total of 1.5 moles of decavanadate per mole of ATPase. Previous measurement of decavanadate binding (Csermely et al., 1985) determined a stoichiometry of 1.5–2 moles of decavanadate per mole of Ca^{2+}-ATPase, which is consistent with our model.

The assignment of this high-density peak to decavanadate leaves only a narrow neck of density (*green line*, Fig. 3, *a,*

TABLE 3 Size of domains in cytoplasmic head of Ca^{2+}-ATPase

			Fraction of cyt. head	
	Sequence	Molecular mass (kDa)	Molecular mass (%)	Volume (%)
P-domain	(234–247, 338–358, 601–750)	19.82	33.5	31.6
A_2-domain*	(376–600)	14.21	24.1	25.5
$A_1+\beta$-domain*	(359–375, 120–233)	24.97	42.3	42.9

*Because the domain boundaries between the A-domain and β-domain were ambiguous, it was not possible to determine their relative masses from the map. However, the uncertainty was confined to the A1 region; A2 was well defined and corresponded in size to the sequence segment following the intron site shown in Fig. 2.

c, f) between the upper and lower parts of the A-domain. These could correspond to the division of the corresponding sequence into A1 and A2 subdomains (see above), the upper region (A1) adjoining the hinge region of the P-domain and the lower region (A2) lining the cavities that bind the nucleotide. Indeed, A2 contains all of the functional sites in the A-domain, and its calculated molecular weight is consistent with the size of this part of the map (Table 3). It is also noteworthy that the internal decavanadate site contacts both parts of the A-domain as well as the P- and β-domains and so is in an ideal position to stabilize their interactions. This stabilization could account for the compact structure of this E_2 form of the pump compared to the E_1Ca_2 form (Stokes et al., 1999).

Docking of dehalogenase core domain into Ca^{2+}-ATPase

Our next step was to dock the atomic structure of the dehalogenase core domain into the yellow density assigned to the Ca^{2+}-ATPase P-domain (Figs. 4 and 5). We tried two different automated methods for docking, but neither produced convincing or consistent results. Docking was therefore done manually, and the general orientation was chosen to be consistent with short connections between the stalk helices S4 and S5 and the ends of the dehalogenase fold, so that the β-strands run away from the membrane. The pattern of density within the P-domain was then used for a more precise positioning of the dehalogenase fold. Generally speaking, α-helices generate relatively strong density peaks at 8 Å resolution, whereas β-strands remain undefined. Thus we positioned α5 and α9 in a plausible region of high density along the back of the P-domain, which also matched α6 to a high-density rod that protrudes from the side of the P-domain. In addition, a low-density region in the P-domain was matched with a low-density region in maps generated from the dehalogenase coordinates between α5, α9, and the β-sheet (Figs. 1 *a* and 6). There were, however, several discrepancies remaining between the two structures, which are not surprising given the large differences in sequence and the probability that extensions of stalk helices S2 and S3 run through this region and thus contribute extra density. In particular, two regions of 1JUD project beyond the yellow envelope of the P-domain. One is the L_{56} loop (Fig. 4 *a*), which is variable among dehalogenases and is predicted to be slightly shorter and α-helical for Ca^{2+}-ATPase (we have remodeled this loop in Fig. 6 to minimize this protrusion). The other is the loop between β3 and α7 (Fig. 4 *c*), which is actually a short 3_{10} helix in the dehalogenase and is two residues shorter in Ca^{2+}-ATPase. On the other hand, there are unassigned densities in the P-domain, the largest being at the bottom of Fig. 4 *c*. This particular density is next to the loop between α6 and β3, which consists of a short 3_{10} helix in the dehalogenase but has an extra 28 residues in Ca^{2+}-ATPase; these extra residues could plausibly fill this unassigned space. We can find no well-resolved connecting density between the β-domain and stalk helices, although chains could be accommodated by adjustments of α8 and L_{56}, which occupy a relatively large, high-density region at the interface with the A-domain (Fig. 3 *d*). Alternatively, the β-domain terminates as a small column of density that resembles a helix (Fig. 3 *d*), and it is possible that it is connected to the stalk by a disordered, and therefore invisible, loop.

DISCUSSION

Modeling of the catalytic site

To evaluate the consistency of this model with the results of mutagenesis and chemical modification, a particular binding configuration for ATP must be specified. Although the active site for nucleophilic attack on the γ-phosphate is defined by the dehalogenase structure, the binding of the rest of the ATP molecule is not, both because it is substantially different from dehalogenase ligands and because the contribution of the subdomain to this binding pocket is currently undefined. Nevertheless, according to our model, the binding pocket for ATP should occur at the interface between the A-domain and the P-domain, and two low-density cavities are seen at this interface (labeled *a* and *b* in Fig. 6, *single* and *double arrowheads* in Fig. 3, *d* and *e*). These two cavities ultimately merge and provide plausible binding pockets for either one or possibly two adenosine ring systems. They are both close enough to the catalytic aspartate (D^{351}) to permit interaction with the γ-phosphate;

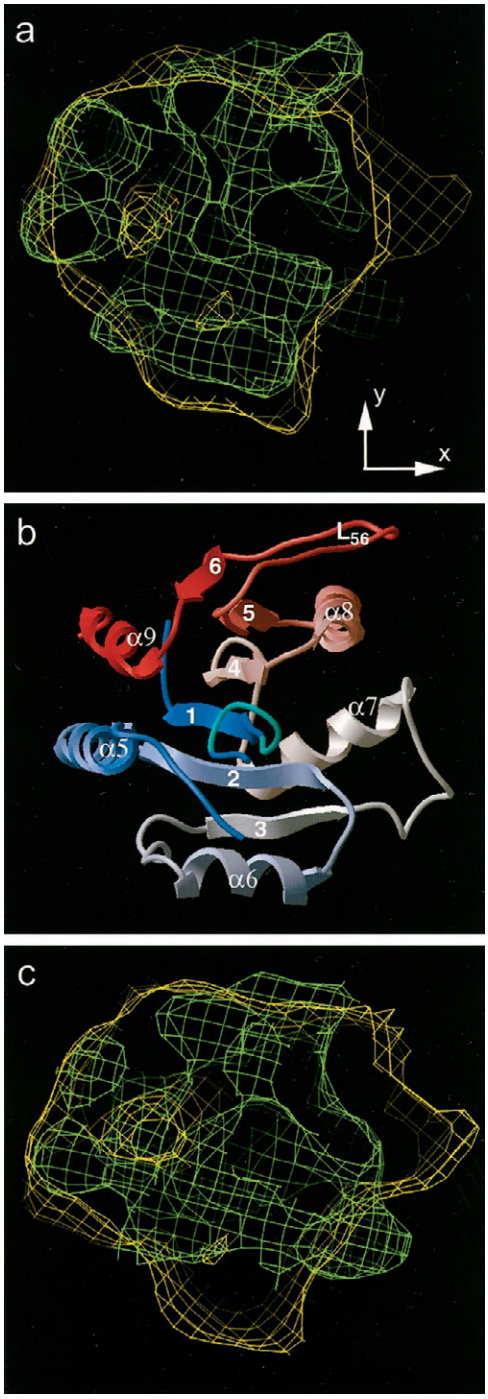

FIGURE 4 Fitting the dehalogenase core domain to the P-domain density from Ca^{2+}-ATPase. The density envelopes from Ca^{2+}-ATPase and dehalogenase are shown in yellow and green, respectively. *a* is from the top of the P-domain (*topmost arrow* in Fig. 3 *a*), whereas *c* is from the bottom (*lower arrow* in Fig. 3 *a*). The ribbon diagram for the entire dehalogenase core domain is shown in *b*, with the same coloring scheme as in Fig. 1. Axes are the same as in Fig. 3.

however, the location of the difference density produced by CrATP is consistent with the position of cavity *a*, even though the two cavities could not be resolved in the corresponding maps because of their lower resolution (Yonekura et al., 1997). Cavity *b* might contribute to a second ATP binding site, for which there is considerable evidence in the literature (see below).

The γ-phosphate itself, which is modeled as a transition state VO_3, occupies an active site at the topological switch point between β-strands 1 and 4; such a switch point is generally favorable for an active site in α/β-type structures (Branden, 1980) and specifically matches the active site of the dehalogenases (Hisano et al., 1996; Ridder et al., 1997). The side chains shown in Fig. 6 correspond to mutation-sensitive residues in Table 2, which have been modeled into the dehalogenase fold. The location of all of these residues at the ligand binding surface, mostly in close juxtaposition with the γ-phosphate, is strongly supportive of our model. In particular, the γ-phosphate is surrounded by four mutationally sensitive residues (D^{351}, D^{703}, D^{707}, K^{684}), whose homologs in the dehalogenase are directly involved in nucleophilic attack on the substrate. The signature sequence for P-type pumps ($DKTGTL^{356}$) is represented by the cyan loop, following β1, which links D^{351} to the hinge and which is stabilized by a continuous network of H-bonds in the dehalogenase structure. The loop following β2 contains D^{627}, which is more distant, but could indirectly affect the disposition of the preceding several residues (T^{625} and G^{626}), which also contribute ligands to the hydrogen-bonding system at the active site of dehalogenases; indeed, these preceding residues constitute the fourth sequence motif that was used to define the superfamily (Aravind et al., 1998). The final residue shown is R^{678} at the C-terminus of β3, whose orientation in Fig. 6 was determined by energy minimization. This residue is located on the surface of the P-domain, pointing toward the A-domain, consistent with its observed cross-linking by glutaraldehyde to K^{492} in the A-domain. The ability of decavanadate to block this cross-link is evidence for the effect of this reagent on domain interactions.

Chemical modification and evidence for two nucleotide binding sites

The binding of nucleotides and nucleotide analogs has been the subject of many types of experiment, and the complexity of the results has given rise to a variety of different explanations. The basic observation is that the high-affinity catalytic site binds ATP with a K_d of ~5 μM to give a phosphoenzyme whose subsequent transformations are further activated by ATP binding at sites of medium (50 μM) and low (1 mM) affinity (e.g., Moller et al., 1980). In other experiments the binding constants for inhibitors or for protection by ATP against irreversible inhibitors have been measured. The simplest explanation (Champeil et al., 1988; Moczydlowski and Fortes, 1981) postulates a single nucleotide site that changes in affinity after phosphorylation of D^{351}, giving rise to low-affinity modulations. Others assume

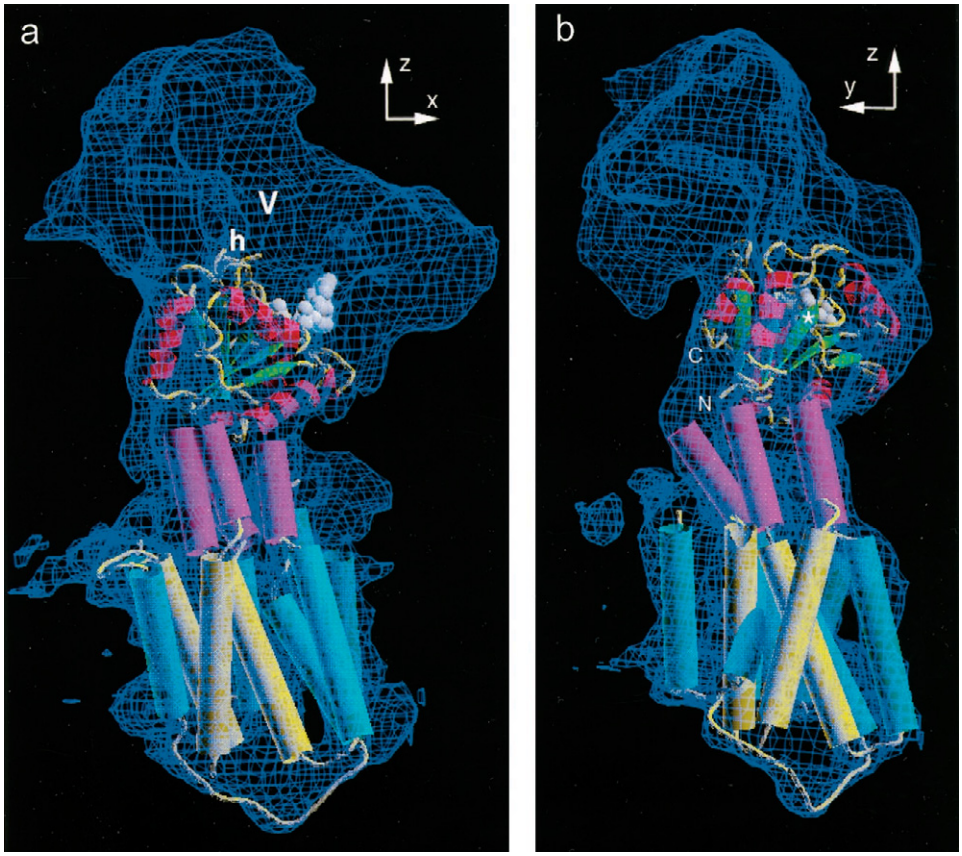

FIGURE 5 New model for the architecture of Ca^{2+}-ATPase, showing transmembrane and stalk helices as well as the P-domain. Transmembrane and stalk domains are as fitted by Zhang et al. (1998) with hypothetical connecting loops. The hinge between the P-domain and A-domain is indicated by h, and the putative decavanadate peak is indicated by V. The N- and C-termini of the P-domain are indicated in *b*, as is the location of the catalytic D^{351} (*star*). Axes are the same as in Figs. 3 and 4.

separate catalytic and regulatory sites, which may be on the same peptide chain (Ward and Cavieres, 1998a) or on opposing chains of a dimeric unit (Linnertz et al., 1998).

Our observation of two cavities at the domain interface is consistent with the existence of two nucleotide sites within a single molecule (*a* and *b* in Fig. 6). Because β-γ-CrATP occupies site *a* and has the same stereochemistry as MgATP (as found in the active sites of myosin and F_1 ATPase), we assume that this is the catalytic ATP site. Site *b* is near K^{678} and extends upward out of the section in Fig. 6. As mentioned, K^{678} can be cross-linked to K^{492} by glutaraldehyde, which in turn can be cross-linked to K^{515} by 4,4′-diisothiocyanostilbene-2,2′-disulfonic acid, suggesting that these three residues are close together. Association with a nucleotide binding site is suggested by the fact that K^{492} is modified by a number of nucleotide analogs and that FITC labeling of K^{515} blocks ATP binding (Table 1). Thus we propose that the well-studied residues K^{492} and K^{515} are associated with site *b* and form a secondary nucleotide binding site.

In fact, there is ample evidence from various ATP analogs that suggest the existence of two nucleotide binding sites that can be simultaneously occupied. For example, although labeling of K^{492} or K^{515} generally blocks phosphorylation by ATP, D^{351} can still react with smaller substrates such as P_i, acetyl phosphate, or *p*-nitrophenyl phosphate (and even, in the Na^+/K^+-ATPase, with *O*-methyl fluorescein phosphate). In addition, nucleotides and their analogs are still able to bind to the labeled enzyme with moderate affinity and inhibit its reactivity with these small substrates, supporting the existence of a site distinct from K^{492} and K^{515} (Champeil et al., 1988; Mignaco et al., 1996; Scheiner-Bobis et al., 1993; Ward and Cavieres, 1998b). One explanation for the complexity of these effects is that reagents bound at the catalytic site *a* produce a conformational change that closes down the secondary site *b*, whereas reagents bound at site *b* have mainly local effects. This explanation is supported by the general observation that the reactivity of K^{492} and K^{515} is blocked when the catalytic site *a* is occupied. Furthermore, the reactivity of 11 of 16 cytoplasmic thiol groups is reduced after ATP binding to the catalytic site (Thorley-Lawson and Green, 1977), but reaction of FITC at the secondary site does not protect thiol groups to any significant extent (N. M. Green, unpublished observations) and does not prevent phosphorylation of D^{351} with P_i or with *p*-nitrophenyl phosphate. Assuming that ATP binds preferentially to the catalytic site, this could explain why direct binding measurements have failed to support the existence of two sites. An inconsistency exists in the large effects of mutations at F^{487} and K^{492} on binding of

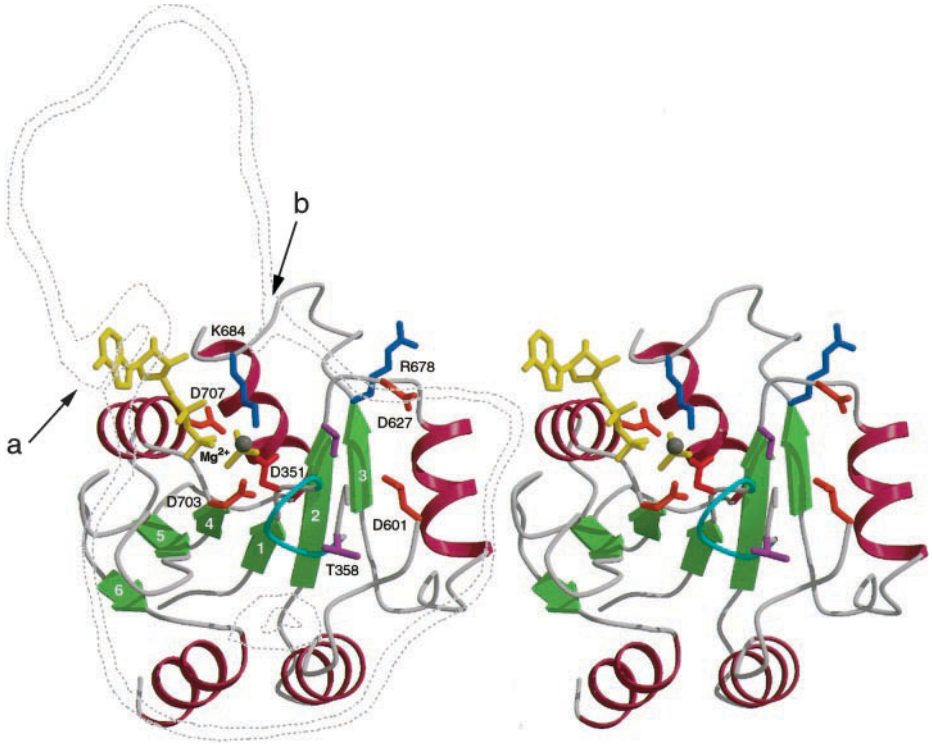

FIGURE 6 Catalytic region of Ca^{2+}-ATPase superimposed on a section from the density map. The section is at the same orientation and position as those of Fig. 3 *d*. For this figure, the pdb file of 1JUD was mutated in Quanta, replacing functional residues in the loops at the ends of β1, β2, β3, and β4 by the corresponding residues of the Ca^{2+}-ATPase (as for Fig. 1). In addition, the L_{56} loop was shortened and remodeled as two turns of helix, based on the predicted secondary structure of the corresponding Ca^{2+}-ATPase sequence. This remodeling would reduce the projection of this loop outside the density envelope of the ATPase as seen in Fig. 4 *a*. ADP-Mg-VO_3 was imported from the structure of myosin (1VOM; Smith and Rayment, 1996) and oriented between D^{351} and site *a* of the density map. Energy minimization of the whole structure was performed using the CHARMm option of Quanta. Only the remodeling of L_{56} required changes in backbone configuration; other changes were restricted to the side chains. The functionally important residues are shown in full, as is R^{678}, which can be cross-linked by glutaraldehyde to the A-domain. The figure was prepared using the program MOLSCRIPT (Kraulis, 1991).

ATP to the catalytic site (McIntosh et al., 1996), but such inconsistencies could be reconciled by postulating ligand-induced domain movements, an idea that is supported by preliminary observations of the Ca^{2+}-bound, E_1 state, discussed below. Moreover, it should be remembered that we do not yet have a 3D structure for the E_1 form and that our structure for the E_2 form includes both decavanadate and thapsigargin, which may influence the relations between the domains.

The multiplicity of binding sites is further extended by our observation of two sites for decavanadate distinct from the CrATP site, both of which remain occupied in the helical arrays containing CrATP (Yonekura et al., 1997). At the same time there is evidence for competition between decavanadate and ATP (Coan et al., 1986), although the data did not allow quantitative conclusions about the dissociation constants. The competition was not caused by orthovanadate, because the latter does not prevent firm binding of ATP (Andersen and Moller, 1985). This implies allosteric interaction between the decavanadate sites and an ATP site, which is also suggested by a decreased decavanadate binding by the FITC derivative of the ATPase (Csermely et al., 1985).

Mechanistic implications of the P-domain structure

This model also provides potential insights into the coupling between sites of phosphorylation and Ca^{2+} transport. Some earlier proposals have emphasized effects transmitted by the direct link between the Ca^{2+} binding site in M4 and the phosphorylation site, while others have considered transport to be the result of more global changes (reviewed by McIntosh, 1998). In our proposed structure, the phosphorylated D^{351} is closely linked to the hinge segment *h1* (TTN^{359}) by the short, fully conserved sequence $KTGTL^{356}$. In the dehalogenase, this connection forms a five-residue loop, which is stabilized by two hydrogen bonds between *i* and *i* + 5 positions. Also according to this analogy, another mutation-sensitive sequence, DPP^{603}, composes the return half of the hinge (segment *h2*) and is linked to TTN^{359} by

two H-bonds. We suggest that this close linking between the $KTGTL^{356}$ loop and the hinge allows changes at the catalytic site to initiate domain movements.

In particular, there is evidence that the bonding of Mg^{2+} changes markedly during the reaction cycle. Previous studies have measured a fall in the rate constant for Mg^{2+} release from 80 s^{-1} in the E·Mg·ATP complex (Reinstein and Jencks, 1993) to less than 0.5 s^{-1} in $E_1{\sim}P{\cdot}Mg(Ca^{2+})_2$ (Wakabayashi and Shigekawa, 1984). This dramatic increase in Mg^{2+} affinity after phosphate transfer and dissociation of ADP suggests that loss of phosphate coordination has been compensated for by new protein ligands with Mg^{2+}. Similar large changes in the Mg^{2+} off-rate accompany phosphorylation from P_i (Ogurusu et al., 1991), and analogous behavior is observed in Na^+/K^+-ATPase, using Co^{2+} as a substitute for Mg^{2+} (Richards, 1988). So far these results have not resulted in any detailed mechanistic proposals, because of lack of a good structural model. However, the H-bond network between the MgATP site and the hinge in our model provides a basis for Mg^{2+}-bonding to initiate movements of the P- and A-domains. Such movements could ultimately be transmitted via the stalk to the Ca^{2+} sites within the membrane.

There are several plausible candidates for Mg^{2+} ligands among the mutation-sensitive sites of Ca^{2+}-ATPase, including T^{353} and T^{355} of the catalytic loop, D^{627}, D^{703}, and D^{707}. A recent structural comparison (Ridder and Dijkstra, 1999) between the catalytic sites of CheY and 1JUD, has suggested D^{351}, D^{703}, and D^{707} as Mg^{2+} ligands. In the related FixJ, the conformational change that accompanies formation of the aspartyl phosphate involved reorientation of T^{625} to bind phosphate together with a 6 Å movement of the histidine corresponding to D^{627} towards the $KTGTL^{356}$ loop (Birck et al., 1999). In Ca^{2+}-ATPase, analogous changes are bound to influence Mg^{2+} bindings as well as the configuration of the hinge region.

The structure of Ca^{2+}-ATPase used for our fitting is likely to represent the E_2 conformation of the enzyme, because crystallization is prevented by Ca^{2+} and promoted by thapsigargin (Stokes and Lacapere, 1994). The binding of Ca^{2+} to the transport site initiates a major structural transition from the E_2 to the E_1 conformation, which activates the catalytic ATP site and leads to nucleophilic attack of D^{351} on ATP. Comparison of the fitted 3D structure with projection images of Ca^{2+}-ATPase in the presence of saturating calcium concentrations (i.e., $E_1{\cdot}Ca_2$; Cheong et al., 1996; Ogawa et al., 1998) and with the structure of H^+-ATPase in the E_1 conformation (Kühlbrandt et al., 1998; Stokes et al., 1999) reveals a substantial rearrangement of the cytoplasmic nose. According to our model, this rearrangement can be explained by a movement of the A-domain relative to the P-domain. In particular, the interface that contains the putative ATP-binding site appears to open up and produce a gap between the domains, perhaps promoting the binding of nucleotide. The two hinge segments between P- and A-domains could provide the necessary flexibility for such a rearrangement. Indeed, analogous domain movements have been shown to modulate the accessibility of the ligand binding site of various structurally related enzymes, such as the family of phosphoribosyl transferases (Smith, 1999). Clearly, revealing the nature of this conformational change is an important step in understanding the structural basis for active transport.

We thank Steve Smerdon for his help with Fig. 6.

This work was supported by National Institutes of Health grant AR40997 to DLS and by the MRC.

REFERENCES

Abagyan, R. A., M. M. Totrov, and D. N. Kuznetsov. 1994. ICM: a new method for protein modeling and design. *J. Comp. Chem.* 15:488–506.

Andersen, J. P. 1995. Dissection of the functional domains of the sarcoplasmic reticulum Ca^{2+}-ATPase by site-directed mutagenesis. *Biosci. Rep.* 15:243–261.

Andersen, J. P., and J. V. Moller. 1985. The role of Mg^{2+} and Ca^{2+} in the simultaneous binding of vanadate and ATP at the phosphorylation site of sarcoplasmic reticulum Ca^{2+}-ATPase. *Biochim. Biophys. Acta.* 815:9–15.

Aravind, L., M. Y. Galperin, and E. V. Koonin. 1998. The catalytic domain of the P-type ATPase has the haloacid dehalogenase fold. *Trends Biol. Sci.* 23:127–129.

Auer, M., G. A. Scarborough, and W. Kühlbrandt. 1998. Three-dimensional map of the plasma membrane H^+-ATPase in the open conformation. *Nature.* 392:840–843.

Axelsen, K. B., and M. G. Palmgren. 1998. Evolution of substrate specificities in the P-type ATPase superfamily. *J. Mol. Evol.* 46:84–101.

Bigelow, D. J., and G. Inesi. 1992. Contributions of chemical derivatization and spectroscopic studies to the characterization of the Ca^{2+} transport ATPase of sarcoplasmic reticulum. *Biochim. Biophys. Acta.* 1113:323–338.

Birck, C., L. Mourey, P. Gouet, B. Fabry, J. Schumacher, P. Rousseau, D. Kahn, and J.-P. Samama. 1999. Conformational changes induced by phosphorylation of the FixJ receiver domain. *Structure*. 7:1505–1515.

Branden, C. I. 1980. Relation between structure and function of alpha/beta-proteins. *Q. Rev. Biophys.* 13:317–338.

Champeil, P., T. Menguy, S. Soulie, B. Juul, A. G. de Gracia, F. Rusconi, P. Falson, L. Denoroy, F. Henao, M. le Maire, and J. V. Moller. 1998. Characterization of a protease-resistant domain of the cytosolic portion of sarcoplasmic reticulum Ca^{2+}-ATPase: nucleotide- and metal-binding sites. *J. Biol. Chem.* 273:6619–6631.

Champeil, P., S. Riollet, S. Orlowski, F. Guillain, C. J. Seebregts, and D. B. McIntosh. 1988. ATP regulation of sarcoplasmic reticulum Ca^{2+}-ATPase. Metal-free ATP and 8-bromo-ATP bind with high affinity to the catalytic site of phosphorylated ATPase and accelerate dephosphorylation. *J. Biol. Chem.* 263:12288–12294.

Cheong, G.-W., H. S. Young, H. Ogawa, C. Toyoshima, and D. L. Stokes. 1996. Lamellar stacking in three-dimensional crystals of Ca^{2+}-ATPase from sarcoplasmic reticulum. *Biophys. J.* 70:1689–1699.

Coan, C., D. J. Scales, and A. J. Murphy. 1986. Oligovanadate binding to sarcoplasmic reticulum ATPase. Evidence for substrate analogue behavior. *J. Biol. Chem.* 261:10394–10403.

Collet, J. F., V. Stroobant, M. Pirard, G. Delpierre, and E. Van Schaftingen. 1998. A new class of phosphotransferases phosphorylated on an aspartate residue in an amino-terminal DXDX(T/V) motif. *J. Biol. Chem.* 273:14107–14112.

Csermely, P., S. Varga, and A. Martonosi. 1985. Competition between decavanadate and fluorescein isothiocyanate on the Ca^{2+}-ATPase of sarcoplasmic reticulum. *Eur. J. Biochem.* 150:455–460.

Day, V. W., W. G. Klemperer, and D. J. Maltbie. 1987. Where are the protons in $H_3V_{10}O_{28}$? *J. Am. Chem. Soc.* 109:2991–3002.

Green, N. M., and D. L. Stokes. 1992. Structural modelling of P-type ion pumps. *Acta Physiol. Scand.* 146:59–68.

Hisano, T., Y. Hata, T. Fujii, J.-Q. Liu, T. Kurihara, N. Esaki, and K. Soda. 1996. Crystal structure of L-2-haloacid dehalogenase from *Pseudomonas* sp. *YL. J. Biol. Chem.* 271:20322–20330.

Huang, S., S. Negash, and T. C. Squier. 1998. Erythrosin isothiocyanate selectively labels lysine464 within an ATP-protectable binding site on the Ca-ATPase in skeletal sarcoplasmic reticulum membranes. *Biochemistry.* 37:6949–6957.

James, P., M. Inui, M. Tada, M. Chiesi, and E. Carafoli. 1989. Nature and site of phospholamban regulation of the Ca^{2+} pump of sarcoplasmic reticulum. *Nature.* 342:90–92.

Kraulis. 1991. MOLSCRIPT—a program to produce detailed and schematic plots of protein structures. *J. Appl. Crystallogr.* 24:946–950.

Kühlbrandt, W., M. Auer, and G. A. Scarborough. 1998. Structure of P-type ATPases. *Curr. Opin. Struct. Biol.* 8:510–516.

Kurihara, T., J. Q. Liu, V. Nardi-Dei, H. Koshikawa, N. Esaki, and K. Soda. 1995. Comprehensive site-directed mutagenesis of L-2-halo acid dehalogenase to probe catalytic amino acid residues. *J. Biochem.* 117: 1317–1322.

Li, Y.-F., Y. Hata, T. Fujii, T. Hisano, M. Nishihara, T. Kurihara, and N. Esaki. 1998. Crystal structures of reaction intermediates of L-2 haloacid dehalogenase and implications for the reaction mechanism. *J. Biol. Chem.* 273:15035–15044.

Linnertz, H., P. Urbanova, T. Obsil, P. Herman, E. Amler, and W. Schoner. 1998. Molecular distance measurements reveal an $(\alpha\beta)_2$ dimeric structure of Na^+/K^+-ATPase. High affinity ATP binding site and K^+-activated phosphatase reside on different alpha-subunits. *J. Biol. Chem.* 273:28813–28821.

MacLennan, D. H., C. J. Brandl, B. Korczak, and N. M. Green. 1985. Amino-acid sequence of a Ca^{2+} + Mg^{2+}- dependent ATPase from rabbit muscle sarcoplasmic reticulum, deduced from its complementary DNA sequence. *Nature.* 316:696–700.

MacLennan, D. H., W. J. Rice, and N. M. Green. 1997. The mechanism of Ca^{2+} transport by sarco(endo)plasmic reticulum Ca^{2+} ATPases. *J. Biol. Chem.* 272:28815–28818.

McIntosh, D. 1998. The ATP binding sites of P-type ion transport ATPases. *Adv. Mol. Cell Biol.* 23A:33–99.

McIntosh, D. B., D. G. Woolley, B. Vilsen, and J. P. Andersen. 1996. Mutagenesis of segment 487Phe-Ser-Arg-Asp-Arg-Lys492 of sarcoplasmic reticulum Ca^{2+}-ATPase produces pumps defective in ATP binding. *J. Biol. Chem.* 271:25778–25789.

Mignaco, J. A., O. H. Lupi, F. T. Santos, H. Barrabin, and H. M. Scofano. 1996. Two simultaneous binding sites for nucleotide analogs are kinetically distinguishable on the sarcoplasmic reticulum Ca^{2+}-ATPase. *Biochemistry.* 35:3886–3891.

Moczydlowski, E. G., and P. A. Fortes. 1981. Inhibition of sodium and potassium adenosine triphosphatase by 2′,3′-*O*-(2, 4, 6-trinitrocyclohexadienylidene) adenine nucleotides. Implications for the structure and mechanism of the Na:K pump. *J. Biol. Chem.* 256:2357–2366.

Moller, J. V., K. E. Lind, and J. P. Andersen. 1980. Enzyme kinetics and substrate stabilization of detergent-solubilized and membranous (Ca^{2+}-Mg^{2+})- activated ATPase from sarcoplasmic reticulum. *J. Biol. Chem.* 255:1912–1920.

Moller, J. V., B. Juul, and M. le Maire. 1996. Structural organization, ion transport, and energy transduction of ATPases. *Biochim. Biophys. Acta.* 1286:1–51.

Murphy, A. J. 1988. Affinity labeling of the active site of the Ca^{2+}-ATPase of sarcoplasmic reticulum. *Biochim. Biophys. Acta.* 946:57–65.

Ogawa, H., D. L. Stokes, H. Sasabe, and C. Toyoshima. 1998. Structure of the Ca^{2+} pump of sarcoplasmic reticulum: a view along the lipid bilayer at 9-Å resolution. *Biophys. J.* 75:41–52.

Ogurusu, T., S. Wakabayashi, and M. Shigekawa. 1991. Activation of sarcoplasmic reticulum Ca^{2+}-ATPase by Mn^{2+}: a Mn^{2+} binding study. *J. Biochem.* 109:472–476.

Perez, C., B. Michelet, V. Ferrant, P. Bogaert, and M. Boutry. 1992. Differential expression within a three-gene subfamily encoding a plasma membrane H^+-ATPase in *Nicotiana plumbaginifolia. J. Biol. Chem.* 267:1204–1211.

Reinstein, J., and W. P. Jencks. 1993. The binding of ATP and Mg^{2+} to the calcium adenosinetriphosphatase of sarcoplasmic reticulum follows a random mechanism. *Biochemistry.* 32:6632–6642.

Richards, D. E. 1988. Occlusion of cobalt ions within the phosphorylated forms of the Na^+-K^+ pump isolated from dog kidney. *J. Physiol. (Lond.).* 404:497–514.

Ridder, I. S., and B. W. Dijkstra. 1999. Identification of the Mg^{2+}-binding site in the P-type ATPase and phosphatase members of the HAD (haloacid dehalogenase) superfamily by structural similarity to the response regulator protein CheY. *Biochem. J.* 339:223–226.

Ridder, I. S., H. J. Rozeboom, K. H. Kalk, D. B. Janssen, and B. W. Dijkstra. 1997. Three-dimensional structure of L-2-haloacid dehalogenase from *Xanthobacter autotrophicus* GJ10 complexed with the substrate-analogue formate. *J. Biol. Chem.* 272:33015–33022.

Rost, B., and C. Sander. 1993. Prediction of protein secondary structure at better than 70% accuracy. *J. Mol. Biol.* 232:584–599.

Scheiner-Bobis, G., J. Antonipillai, and R. A. Farley. 1993. Simultaneous binding of phosphate and TNP-ADP to FITC-modified Na^+,K^+-ATPase. *Biochemistry.* 32:9592–9599.

Smith, C. A., and I. Rayment. 1996. X-ray structure of the magnesium(II). ADP.vanadate complex of the *Dictyostelium discoideum* myosin motor domain to 1.9 Å resolution. *Biochemistry.* 35:5404–5417.

Smith, J. L. 1999. Forming and inhibiting PRT active sites. *Nature Struct. Biol.* 6:502–504.

Stokes, D. L., M. Auer, P. Zhang, and W. Kuehlbrandt. 1999. Comparison of H^+-ATPase and Ca^{2+}-ATPase suggests that a large conformational change initiates P-type ion pump reaction cycles. *Curr. Biol.* 9:672–679.

Stokes, D. L., and J.-J. Lacapere. 1994. Conformation of Ca^{2+}-ATPase in two crystal forms: effects of Ca^{2+}, thapsigargin, AMP-PCP, and Cr-ATP on crystallization. *J. Biol. Chem.* 269:11606–11613.

Taylor, W. R., and N. M. Green. 1989. The predicted secondary structures of the nucleotide-binding sites of six cation-transporting ATPases lead to a probable tertiary fold. *Eur. J. Biochem.* 179:241–248.

Thorley-Lawson, D. A., and N. M. Green. 1977. The reactivity of the thiol groups of the adenosine triphosphatase of sarcoplasmic reticulum and their location on tryptic fragments of the molecule. *Biochem J.* 167: 739–748.

Toyoshima, C., H. Sasabe, and D. L. Stokes. 1993. Three-dimensional cryo-electron microscopy of the calcium ion pump in the sarcoplasmic reticulum membrane. *Nature.* 362:469–471.

Tran, C. M., E. E. Huston, and R. A. Farley. 1994. Photochemical labeling and inhibition of Na, K-ATPase by 2-azido-ATP. *J. Biol. Chem.* 269: 6558–6565.

Tumer, Z., B. Vural, T. Tonnesen, J. Chelly, A. P. Monaco, and N. Horn. 1995. Characterization of the exon structure of the Menkes disease gene using vectorette PCR. *Genomics.* 26:437–442.

Wakabayashi, S., and M. Shigekawa. 1984. Role of divalent cation bound to phosphoenzyme intermediate of sarcoplasmic reticulum ATPase. *J. Biol. Chem.* 259:4427–4436.

Ward, D. G., and J. D. Cavieres. 1998a. Affinity labeling of two nucleotide sites on Na, K-ATPase using 2′(3′)-*O*-(2,4,6-trinitrophenyl)8-azidoadenosine 5′-[α-^{32}P]diphosphate (TNP-8N_3-[α-^{32}P]ADP) as a photoactivatable probe. Label incorporation before and after blocking the high affinity ATP site with fluorescein isothiocyanate. *J. Biol. Chem.* 273:33759–33765.

Ward, D. G., and J. D. Cavieres. 1998b. Photoinactivation of fluorescein isothiocyanate-modified Na, K-ATPase by 2′(3′)-*O*-(2,4,6-trinitrophenyl)8-azidoadenosine 5′-diphosphate. Abolition of E1 and E2 partial reactions by sequential block of high and low affinity nucleotide sites. *J. Biol. Chem.* 273:14277–14284.

Yonekura, K., D. L. Stokes, H. Sasabe, and C. Toyoshima. 1997. The ATP-binding site of Ca^{2+}-ATPase revealed by electron image analysis. *Biophys. J.* 72:997–1005.

Zhang, P., C. Toyoshima, K. Yonekura, N. M. Green, and D. L. Stokes. 1998. Structure of the calcium pump from sarcoplasmic reticulum at 8 Å resolution. *Nature.* 392:835–839.